The Journal of Chemical Physics

RESEARCH ARTICLE | APRIL 14 2026

Specific ion effects on long-range correlations of amino acids in aqueous solution from experimental and computational dielectric spectra

Special Collection: Computational Spectroscopy

Marion Sappl ; Christian Fellinger ; Amala Elizabeth ; Dimitra Kanta ; Leon Prädel; Johannes Hunger ; Christian Schröder ; Vasileios Balos

J. Chem. Phys. 164, 144508 (2026)
https://doi.org/10.1063/5.0319199

The Journal of Chemical Physics ARTICLE pubs.aip.org/aip/jcp

Specific ion effects on long-range correlations of amino acids in aqueous solution from experimental and computational dielectric spectra

Cite as: J. Chem. Phys. 164, 144508 (2026); doi: 10.1063/5.0319199
Submitted: 23 December 2025 • Accepted: 23 March 2026 •
Published Online: 14 April 2026

Marion Sappl,[1,2] Christian Fellinger,[3,4] Amala Elizabeth,[5] Dimitra Kanta,[5] Leon Prädel,[5] Johannes Hunger,[5,a)] Christian Schröder,[1,a)] and Vasileios Balos[6,a)]

AFFILIATIONS

[1] Department of Computational Biological Chemistry, Faculty of Chemistry, University of Vienna, Währinger Str. 17, 1090 Vienna, Austria
[2] Vienna Doctoral School in Chemistry (DoSChem), University of Vienna, Währinger Str. 42, 1090 Vienna, Austria
[3] Department of Pharmaceutical Sciences, Faculty of Life Sciences, University of Vienna, Josef-Holaubek-Platz 2, 1090 Vienna, Austria
[4] Vienna Doctoral School of Pharmaceutical, Nutritional and Sport Sciences (VDS PhaNuSpo), University of Vienna, Josef-Holaubek-Platz 2, 1090 Vienna, Austria
[5] Max-Planck Institute for Polymer Research, Ackermannweg 10, 55128 Mainz, Germany
[6] Instituto Madrileño de Estudios Avanzados en Nanociencia (IMDEA Nanociencia), C/Faraday 9, 28049 Madrid, Spain

Note: This paper is part of the Special Topic on Computational Spectroscopy.

[a)] **Authors to whom correspondence should be addressed:** hunger@mpip-mainz.mpg.de; christian.schroeder@univie.ac.at; and vasileios.balos@imdea.org

ABSTRACT

Specific ion effects are often unpredictable in their manifestation within collective behavior, as the underlying principles of how they mediate water–solute interactions remain unclear. In this study, we investigate the influence of simple ions on amino acids in electrolyte solutions, focusing on arginine, lysine, and serine in potassium iodide, potassium bromide, potassium chloride, sodium chloride, and lithium chloride solutions. We combine experimental techniques and molecular dynamics simulations to examine how monovalent ions affect the dielectric spectra of these complex solutions. Our results reveal three key effects of salt addition: (I) A decrease in the permittivity of the solution, a phenomenon known as the dielectric decrement, which is phenomenologically described by the Langevin function. The extent of the dielectric decrement is dependent on the specific ion. (II) An increase in the relaxation time of amino acids. Furthermore, the relaxation time of water is either increased or decreased depending on the specific salt–amino acid combination. The extent of the change in relaxation time compared to binary mixtures is dependent on the charge density of the added ions. (III) Long-range restructuring of amino acids and water leads to changes in their relative orientation over large distances. These findings provide new insights into how ions affect water–amino acid interactions and their impact on the dielectric properties of electrolyte solutions.

I. INTRODUCTION

Specific ion effects in aqueous solutions, often framed in terms of the Hofmeister series, play a central role in controlling the solubility, stability, and phase behavior of a wide range of chemical and biological systems.[1–5] Classic manifestations include salting-in and salting-out phenomena, where the addition of salt either increases or decreases the solubility of macromolecules, surfactants, or small amphiphiles. Although such effects have been known for more than a century, a unified microscopic picture of how different ions modulate the structure and dynamics of water and solutes is still lacking.[6,7] The pioneering work of Hofmeister in the late nineteenth century[8] established a phenomenological ordering of ions according to their ability to precipitate proteins and other solutes. Later studies showed that the polarity and surface charge density of both cations and anions are key determinants of whether salts promote aggregation ("salting-out") or enhanced solubility ("salting-in").[9,10]

A substantial body of work has sought to rationalize specific ion effects in terms of ion size, charge density, and hydration properties, and to disentangle direct ion–solute interactions from more delocalized, water-mediated mechanisms.[7,11–13] Experimental and simulation studies have emphasized that ions can interact directly with charged or polar functional groups,[14–16] but they can also act indirectly by reorganizing the hydrogen-bond network of water and thereby modifying collective polarization and dielectric properties.[7,12,13,17,18] The balance between these contributions is system-dependent and remains an active area of research.

Aqueous solutions of single amino acids provide a particularly convenient model platform to probe ion-specific effects at the level of well-defined, chemically simple solutes. They retain key functional motifs (e.g., charged and polar side chains) found in peptides and proteins but avoid the structural and dynamical complexity of full macromolecules. Specific ion effects have been reported, for example, in the ion-specific solubility of amino acids,[19] in the coordination patterns of ions around amino acid side chains,[20,21] and in the dependence of these features on the chosen force field in simulations.[20] Previous studies generally suggest that many Hofmeister-type trends can be sufficiently rationalized at the level of direct ion–amino acid interactions, while water restructuring plays a more subtle, system-dependent role.[2,19–21] More recently, the influence of ions on the permittivity of electrolyte solutions has highlighted the importance of cross-correlations between hydration water and bulk-like water and the impact of long-range salt effects on water structure and dynamics.[22]

In this study, we investigate specific ion effects in ternary aqueous mixtures of amino acids and simple monovalent salts, with a particular focus on how ions modulate long-range dipolar correlations and collective dielectric properties. We combine broadband dielectric relaxation spectroscopy with molecular dynamics (MD) simulations to resolve the contributions of water and amino acids to the dielectric spectra and to disentangle self- and cross-correlation terms. Using OpenMM[23] with an adapted AMBER force field based on ff14SB,[24] we characterize how ion identity and charge density affect the dielectric decrement, relaxation times, and orientational correlations in solutions of arginine, lysine, and serine. Rather than directly addressing the full complexity of protein (de)stabilization, our aim is to provide a microscopic description of ion-specific effects in amino acid-based model systems that underlie salting-in and salting-out behavior at a more coarse-grained level.

II. METHODS

A. Composition of the binary aqueous and ternary electrolyte amino acid mixtures

To characterize the dielectric properties of amino acids in solution, two distinct sets of aqueous samples were prepared: (i) binary aqueous solutions of arginine (Arg), lysine (Lys), and serine (Ser) and (ii) ternary solutions consisting of water, amino acids, and added salts.

Binary aqueous solutions of amino acids were prepared volumetrically using Milli-Q water. The amino acids (Karl Roth GmbH) were used as received. Concentration ranges were chosen based on solubility limits and were as follows: Arg at 0.1, 0.2, 0.3, 0.4, and 0.5 mol L^{-1}; Lys at 1, 2, and 3 mol L^{-1}; and Ser at 0.5, 1.0, 1.5, 2.0, 2.5, and 3.0 mol L^{-1}. These amino acids were selected due to the distinct nature of their side chains: Arg and Lys possess positively charged side chains, whereas Ser has a polar side chain.[25,26] The charge state of the amino acids in the solution was determined through pH measurements [see supplementary material, Sec. SI.A. and Fig. S1(a)]. The pH values were close to their respective isoelectric points, indicating the presence of amino acids in their zwitterionic form.[27] Note that under these conditions, the positive charge is located on the side chains of Arg and Lys.

Further investigations into specific ion effects were conducted by preparing a second series of ternary samples with the amino acids dissolved in water at varying salt concentrations. The concentration of each amino acid was maintained constant and at levels high enough to ensure reliable detection of their dielectric response, yet below their solubility limits: 0.45 mol L^{-1} for Arg, 1.0 mol L^{-1} for Lys, and 1.0 mol L^{-1} for Ser. We prepared ternary solutions with different molar ratios, with a maximum molar ratio of ~2:1 salt to amino acid. For the study of cation-specific effects, chloride salts of potassium K^+, sodium Na^+, and lithium Li^+ were utilized, as well as a potassium iodide KI solution to examine the influence of a highly denaturing anion, such as iodide. All samples were prepared in a glovebox by weighing the required amounts of amino acids and salt into volumetric flasks to prevent moisture uptake, followed by filling to volume with Milli-Q water.

In addition, KBr was used in our MD simulations, but we chose only KCl and KI for experimental measurements, as the anionic effects on the dielectric spectra were less pronounced than the effects of the cation. We chose potassium halide salts at the end of the scales, from chaotropic to kosmotropic, to compare the results with our simulations. Chloride and potassium were selected as common counterions, as both are considered unlikely to destabilize proteins.[28,29] The pH remained relatively unaffected by the addition of salt [see supplementary material, Fig. S1(b)], suggesting that salt addition does not significantly alter the charge state of the amino acids. The concentrations of the amino acids used in the simulations matched those used in the experiments, and we used similar salt concentrations without added salt up to a 2:1 molar ratio of salt to amino acid. Section SVII in the supplementary material provides

details regarding the simulation setup and the non-polarizable force field.

B. Interpretation of dielectric spectra from experiments and molecular dynamics

We investigated specific ion effects on amino acids in solution using dielectric relaxation spectroscopy,[30,31] which probes the sample polarization under an external alternating electric field with varying frequencies ν. Predominantly at microwave frequencies, the frequency-dependent polarization arises from the field-induced orientation of the molecules' permanent dipole moments. Complex permittivity spectra were measured using a combination of three different experiments: Frequencies at 0.30 GHz $\leq \nu \leq$ 0.51 GHz were covered using coaxial probes made from SMA hermetic feedthroughs, while frequencies at 0.54 GHz $\leq \nu \leq$ 53 GHz were covered using a frequency domain reflectometer based on an Anritsu Vector Star MS4647A vector network analyzer with an open-end coaxial probe based on 1.85 mm coaxial connectors.[15] For covering frequencies at 56 GHz $\leq \nu \leq$ 125 GHz, we analogously used an open-end coaxial probe based on 1 mm coaxial connectors combined with an external frequency converter module (Anritsu 3744A mmW module).[15] Note that for the binary samples, only the two high-frequency probes were used, covering the regions: 0.33 GHz $\leq \nu \leq$ 36 GHz and 56 GHz $\leq \nu \leq$ 125 GHz. To accurately model the experimental dielectric spectrum, after removing the contribution from the conductivity, we employed a Debye relaxation model to describe the amino acid relaxation and a Cole–Cole[32] model to account for the water mode:

$$\varepsilon(\nu) - \varepsilon_\infty = \frac{\varepsilon_R^A}{1 + 2\pi i\nu\,\tau^A} + \frac{\varepsilon_R^W}{1 + (2\pi i\nu\,\tau^W)^{1-\alpha}}. \tag{1}$$

The amplitudes ε_R^A and ε_R^W are the contributions of the amino acid and water to the static permittivity, respectively. In addition, both modes contain a relaxation time τ for the respective amino acid and water contributions to the dielectric spectrum. This approach also effectively captures the symmetric broadening (characterized by the parameter α) of the water relaxation observed in aqueous salt solutions.[33–35]

The computational, frequency-dependent permittivity $\varepsilon(\nu)$ can be calculated from equilibrium MD simulations via the collective dipole moment $\vec{M}_D$:[36,37]

$$\varepsilon(\nu) - \varepsilon_\infty = \frac{1}{3Vk_BT\varepsilon_0}\,\mathcal{L}\left[-\frac{d}{dt}\left\langle \vec{M}_D(0)\cdot\vec{M}_D(t)\right\rangle\right], \tag{2}$$

The Fourier–Laplace transform $\mathcal{L}[\ldots]$ converts the time derivative of the correlation function into a frequency-dependent spectrum. Spectra computed from $\vec{M}_D(t)$ represent a simplified description that accounts solely for the dipolar response. In experimental dielectric spectra, however, additional contributions arising from electrical conductivity are typically present and are subtracted during data processing. Such conductivity effects are likewise not captured by the computational spectra derived from $\vec{M}_D(t)$. A more detailed discussion of the spectral computation is provided in the supplementary material, Sec. SII. For completeness, the corresponding experimental and computational conductivities are shown in Fig. S5 of the supplementary material.

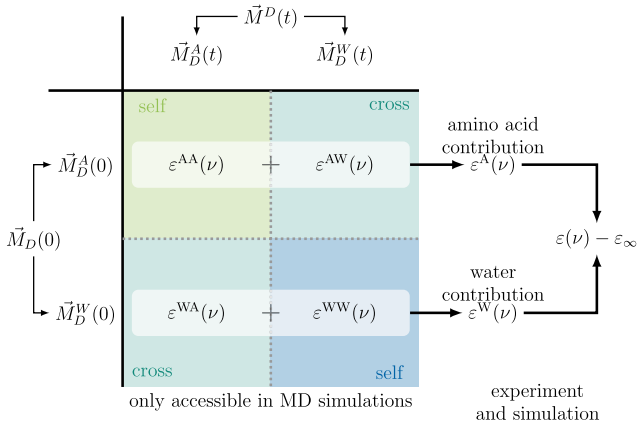

FIG. 1. The collective rotational dipole moment $\vec{M}_D(t)$ can be decomposed into contributions from the amino acid $\vec{M}_D^A(t)$ and water $\vec{M}_D^W(t)$. The Laplace transform of the self- and cross-correlation of the latter two yields the contributions to the dielectric spectrum (green and blue areas for amino acids and water, respectively, and turquoise areas for the cross terms). These individual contributions are accessible only from the simulations. The respective sums of the self- and cross-contributions yield the contributions for the amino acid and water. Their dominant spectral contributions are usually separated in the frequency domain.

The collective rotational dipole moment $\vec{M}_D(t)$ consists of contributions from the amino acids $\vec{M}_D^A(t)$ and the water molecules $\vec{M}_D^W(t)$, as the ions themselves do not possess a dipole moment because they are isotropic and nonpolarizable. These two components give rise to two autocorrelation ($i = j$) functions $C^{ii}(t)$ and two cross-correlation functions $C^{ij}(t)$ for $j \neq i$:

$$C^{ij}(t) = \left\langle \vec{M}_D^i(0)\cdot\vec{M}_D^j(t)\right\rangle, \tag{3}$$

$$\varepsilon^{ij}(\nu) = \frac{1}{3Vk_BT\epsilon_0}\,\mathcal{L}\left[-\frac{dC^{ij}(t)}{dt}\right] = \varepsilon^{ji}(\nu), \tag{4}$$

$$\varepsilon_R^{ij} = \lim_{\nu\to 0}\varepsilon^{ij}(\nu) = \varepsilon_R^{ji}. \tag{5}$$

The Laplace transform of the negative time derivative of each correlation function yields the corresponding contribution $\varepsilon^{ij}(\nu)$ to the dielectric spectrum, as illustrated in Fig. 1 and expressed in Eq. (4). Since the correlation functions are "even" with respect to time, $C^{ij}(t)$ equals $C^{ji}(t)$ and, consequently, $\varepsilon^{ij}(\nu) = \varepsilon^{ji}(\nu)$. The static relative permittivity ε_R^{ij} is the zero-frequency limit of the permittivity. In practice, these individual components (colored areas in Fig. 1) can be distinguished only in MD simulations. Experimentally, only the total spectrum can be resolved. Fitting the spectra to contributions of different species often disregards the mixed contributions of $\varepsilon^{ij}(\nu)$, where $i \neq j$. Usually, these contributions are minimal, and a two-peak fit is sufficient. We combined the contributions of $\varepsilon^{ii}(\nu)$ and $\varepsilon^{ij}(\nu)$, where $i \neq j$, from the simulations to be able to compare computational with experimental results. We define the total amino acid contribution as $\varepsilon^A(\nu) = \varepsilon^{AA}(\nu) + \varepsilon^{AW}(\nu)$, and the water contribution as $\varepsilon^W(\nu) = \varepsilon^{WW}(\nu) + \varepsilon^{WA}(\nu)$. These two dielectric components correspond to the frequency-dependent response of the collective rotational dipole moment of either the amino acids $\vec{M}_D^A(t)$ or the

water molecules $\vec{M}_D^{\mathrm{W}}(t)$ with respect to the total collective rotational dipole moment $\vec{M}_D(t)$:

$$\varepsilon^A(\nu) = \frac{1}{3Vk_BT\varepsilon_0}\mathcal{L}\left[-\frac{d}{dt}\left\langle \vec{M}_D^{\mathrm{A}}(0)\cdot\vec{M}_D(t)\right\rangle\right], \tag{6}$$

$$\varepsilon^W(\nu) = \frac{1}{3Vk_BT\varepsilon_0}\mathcal{L}\left[-\frac{d}{dt}\left\langle \vec{M}_D^{\mathrm{W}}(0)\cdot\vec{M}_D(t)\right\rangle\right]. \tag{7}$$

Although the atomic ions do not directly contribute to the permittivity $\varepsilon(\nu)$, they influence the rotation of the amino acids and water molecules as well as their mutual orientations. Therefore, $\varepsilon^A(\nu)$ and $\varepsilon^W(\nu)$ are functions of the salt species and its concentration.

The time correlation functions $C^{ij}(t)$ in Eq. (3) were fitted using a Kohlrausch–Williams–Watts (KWW) stretched exponential function:

$$C^{ij}(t) = C_0^{ij}\cdot\exp\left[-(t/\tau_{kww}^{ij})^{\beta^{ij}}\right], \tag{8}$$

where β can assume values between 0 and 1 and is the parameter related to the stretching of the exponential function. The frequency domain of a process fitted with a KWW function can be described by the Havriliak–Negami (HN) function:[36,38]

$$\mathcal{L}\left[-\frac{d}{dt}C_0^{ij}\cdot e^{-(t/\tau^{ij})^{\beta^{ij}}}\right] \simeq \frac{C_0^{ij}}{(1-(i\,\omega\,\tau_{\mathrm{HN}}^{ij})^{\alpha_{\mathrm{HN}}^{ij}})^{\gamma_{\mathrm{HN}}^{ij}}}. \tag{9}$$

To transform the KWW parameter to the HN parameter, we used two parameter sets depending on the relaxation times of the species. In the low-frequency region (τ = 100 ps to τ = 900 ps), the parameter τ_{HN} was obtained using the parameters of the KWW fit and the relations of Schröder and Steinhauser.[36] For the high-frequency region, we used the relation suggested by Alvarez *et al.*:[38]

$$\ln\left[\frac{\tau_{\mathrm{HN}}}{\tau_{\mathrm{KWW}}}\right] = 2.6\cdot\sqrt{1-\beta}\cdot\exp\left[-3\beta\right]. \tag{10}$$

The parameters α_{HN} and γ_{HN} were all calculated from the relations of Ref. 36. The KWW relaxation time τ_{KWW} can be transformed into an average relaxation time, which is a connecting parameter between the KWW and HN relaxation times:[38,39]

$$\tau^{ij} = \frac{\Gamma[1/\beta^{ij}]}{\beta^{ij}}\,\tau_{\mathrm{KWW}}^{ij}. \tag{11}$$

III. SPECTRAL PROPERTIES

In Fig. 2(a), we present the experimental dielectric spectrum of a 0.5 mol L^{-1} arginine solution in water. Two overlapping relaxation processes are observable: a lower-frequency relaxation centered around ~0.8 GHz and a higher-frequency relaxation near 20 GHz. Each relaxation is characterized by a peak in the dielectric loss spectrum and a corresponding dispersion in the dielectric permittivity spectrum. The higher-frequency peak is commonly observed for aqueous solutions and is attributed to the collective relaxation of water molecules.[40–42] The lower-frequency peak is commonly

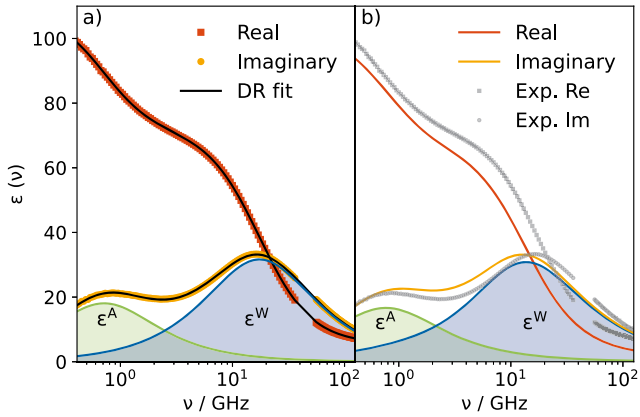

FIG. 2. (a) Experimental dielectric permittivity (orange squares) and dielectric loss (yellow circles) spectra for a solution of 0.5 mol L^{-1} arginine. The black lines show fits using the relaxation model described in Eq. (1). The shaded areas show the contribution of the main water mode at ~20 GHz (blue) and the relaxation of arginine centered at ~0.8 GHz (green) to the dielectric loss. (b) Corresponding computational dielectric spectrum. The orange line shows the computational permittivity in comparison to the experiment (gray squares). The yellow line shows the computational loss spectrum in comparison to the experiment (gray circles). The green and blue areas show the computational contributions to the loss spectrum of arginine and water, respectively.

associated with the orientational relaxation of zwitterionic amino acids.[41,43] This double-peak approach in Eq. (1) describes all experimental spectra at all studied concentrations (see supplementary material, Fig. S3 for the other amino acids and concentrations).

Figure 2(b) displays the corresponding computational spectrum. In principle, two strategies are available for fitting the correlation functions underlying the total spectra. Here, we adopt an approach in which each contribution $C^{ij}(t)$ is fitted individually and subsequently transformed into the corresponding spectral component $\varepsilon^{ij}(\nu)$. The auto- and cross-correlation terms are then combined to yield the total contributions $\varepsilon^W(\nu)$ and $\varepsilon^A(\nu)$. The alternative strategy of fitting $C^A(t)$ and $C^W(t)$ as single effective terms results in an oversimplified description, as it merges distinct dynamical processes into a single fit. This procedure distorts the extracted relaxation times, most notably for water. In particular, the cross-term ε^{AW} is closer in frequency to ε^{AA} than to ε^{WW}, which leads to systematically overestimated relaxation times. By constructing the spectra from individually fitted terms, our approach enables a consistent comparison between experimental and simulated spectral contributions while preserving the underlying relaxation mechanisms. As a result, each species exhibits only one distinct peak in the dielectric spectrum, enabling a straightforward comparison with the experimental data: the low-frequency $\varepsilon''(\nu)$ peak stems from the collective rotation of the amino acid, whereas the high-frequency peak characterizes the water dynamics, as expected. In addition, the computational spectrum in Fig. 2(b) agrees very well with the experimental spectrum over the complete frequency range, validating the applied force field and also confirming that the simulation covers all rotational processes over several orders of magnitude in time.

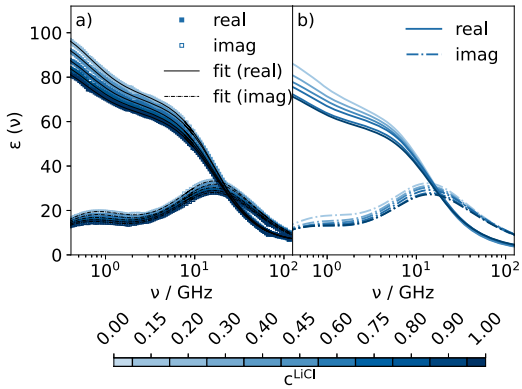

FIG. 3. (a) Experimental dielectric permittivity (closed symbols) and dielectric loss spectra (open symbols) of ternary aqueous solutions of arginine at 0.45 mol L^{-1} with varying LiCl concentration. The black lines show fits using the relaxation model described in Eq. (1). (b) Corresponding dielectric permittivity (solid line) and loss spectra (dash-dotted line) from simulations.

A. Impact of the nature of the salt and its concentration

After the characterization of the dielectric properties of pure amino acids in aqueous solutions, we investigated the specific influence of ionic additives on these systems. As previously discussed, the contributions of the ions themselves cannot be observed in the spectrum as distinct peaks. However, they mediate the interactions of amino acids and water and influence their relaxation processes indirectly. Figure 3 presents the dielectric spectra of Arg in the presence of increasing concentrations of LiCl. The experimental results in Fig. 3(a) clearly show that Eq. (1) provides an excellent description of the dielectric response for these ternary mixtures, as the ions themselves do not exhibit distinct spectral features in the probed frequency range. This observation holds consistently for all other amino acids and salts studied, as illustrated by the respective spectra in Figs. S6–S8, left columns in the supplementary material. The computational spectra in Fig. 3(b) and Figs. S6–S8, right columns in the supplementary material show very good agreement with the experimental data. The theoretical spectra are derived from the frequency-dependent dielectric permittivity $\varepsilon(\nu)$ without explicit contributions from ionic motions, such as local librations of ions within their cages. Both the experimental and computational conductivity increase with increasing salt concentration across all investigated systems (see supplementary material, Fig. S5). These results suggest that, apart from the static conductivity, there is no significant direct contribution to the spectra from the ions. The increase in conductivity can be attributed to the increased number of mobile charge carriers upon the addition of salt.

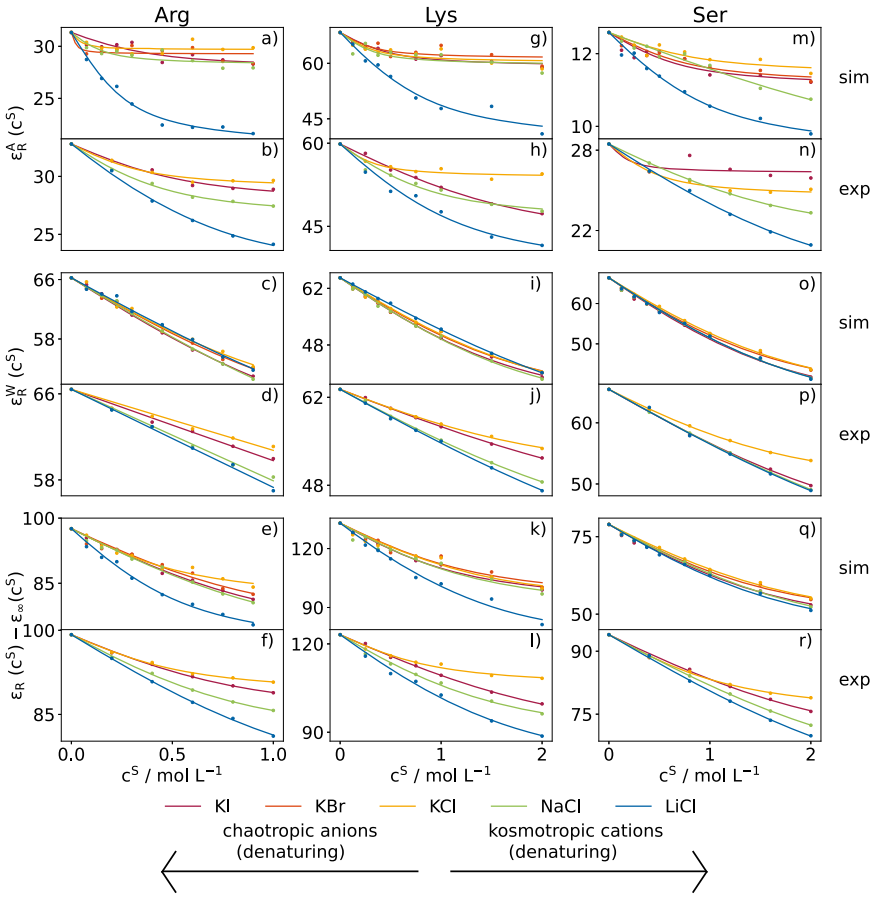

FIG. 4. Comparison of the contributions to the static dielectric permittivity of the rotational collective dipole moment: (a)–(f) from arginine solutions, (g)–(l) from lysine solutions, and (m)–(r) from serine solutions. ε_R^A indicates the contribution to the dielectric permittivity from the amino acids, ε_R^W from water, and $\varepsilon_R(c^S) - \varepsilon_\infty(c^S)$ is the total permittivity. The top graph of each block shows the results from simulations, and the bottom shows the results from experiments.

Although the addition of salts does not produce distinct peaks in the dielectric spectra, it nonetheless exerts a pronounced influence on the interactions between water molecules and amino acids. This influence manifests as modified dynamical behavior of the amino acids and their surrounding hydration shells, as well as water in the hydration shells around the ions. One representative example is the broadening of the water relaxation peak, which corresponds to an increase in the α-parameter in Eq. (1) (see supplementary material, Fig. S9). The most striking observation, however, is the dielectric decrement—the decrease of ε_R with increasing salt concentration—as consistently observed in experiments and simulations. The dielectric decrement of aqueous solutions with increasing salt concentration has been reported for the past century, especially in aqueous solutions.[22,44,45] To explore ion-specific effects on dipolar correlations, we dissect the dielectric decrement of ternary solutions into individual contributions of dipolar species to the total permittivity. In the experimental analysis, the individual dielectric contributions of amino acids and water were determined according to Eq. (1). In the simulations, these quantities were obtained from Eqs. (6) and (7), respectively. The dependencies on the salt concentration c^S are illustrated in Fig. 4, where the upper part of each panel depicts the simulation result and the lower part depicts the corresponding experimental data. The upper panels are the contributions of the amino acids; the middle panels are the contributions of water. The bottom panels depict the total dielectric decrement $\varepsilon_R(c^S) - \varepsilon_\infty(c^S)$. The high-frequency limit $\varepsilon_\infty = 1$ in molecular dynamics simulations[46–48] is described by

$$\frac{\varepsilon_\infty - 1}{\varepsilon_\infty + 2} = \frac{4\pi}{3} \cdot \frac{\alpha}{V}, \tag{12}$$

where α is the total polarizability, which is zero for our non-polarizable simulations and is independent of the salt and concentration. However, the experimental ε_∞ is a fit parameter and consequently varies.

Across all examined amino acids and salt concentrations, a consistent decrease in the dielectric constant is observed. This observation extends to its individual components, namely the dielectric contributions of the amino acid, ε_R^A, and of water, ε_R^W. The magnitude of the dielectric decrement depends systematically on the specific salt species, reflecting ion-specific effects on the local solvent structure and dynamics. This phenomenon, commonly referred to as the dielectric decrement, is well established in the literature.[45,49–52] It arises from the perturbation of the solvent's dielectric response by dissolved ions, which restricts molecular reorientation and polarization. While the dielectric decrement has traditionally been discussed in terms of the overall permittivity of electrolyte solutions, our results demonstrate that this effect also manifests in the decomposed contributions. Specifically, both the amino acid and water components exhibit a distinct dielectric decrement upon salt addition, the magnitude of which depends on the identity of the salt.

The chaotropic iodide anion, well known for its protein-denaturing properties, induces only a modest dielectric decrement of the amino acid contribution [red curve in Figs. 4(a), 4(g), and 4(m) (sim) and Figs. 4(b), 4(h), and 4(n) (exp)] compared to the least denaturing salt, potassium chloride (yellow curve). A notable exception arises in the case of KI with serine, where the amplitude reduction is unexpectedly weaker than that observed for KCl in the experiment [Fig. 4(n)]. The nature of the cation plays a more pronounced role. Exchanging potassium (yellow curve) for sodium (green curve) yields moderate changes in both the computational and experimental dielectric response. However, substitution with the strongly kosmotropic lithium cation (blue curve) leads to a substantial reduction in the dielectric contribution of the amino acid, consistently observed in both simulation and experiment. Replacing the anion alters the dielectric permittivity of the amino acid less than the variation of the cation, suggesting that anion substitution exerts only a minor influence on the rotational dynamics of amino acids.

The dielectric contribution of water also consistently decreases with increasing salt concentration across all investigated salts. Notably, this reduction follows a more linear trend compared to the corresponding decrease observed for the amino acid contribution. Experimentally, the trends are similar to the trends of the contributions of the amino acids. The more denaturing the ions, the higher the decrease in permittivity, with cations appearing to exert a stronger effect. The trends from simulation data are very similar across all salts; however, the trends are not always visibly ordered in the same manner as in experiments. The decline in permittivity can be rationalized by a combination of dilution effects, ion hydration, and kinetic depolarization.[49,53,54] While the more pronounced dielectric decrement of water with KI compared to KCl can be partially explained by the lower molar volume of water in the solution, it is not as obvious for the dielectric decrement of the amino acid. The molar volume of the amino acid does not change with the salt concentration, yet the larger anion with lower charge density I^- has a stronger effect on the contribution of the amino acid to the dielectric permittivity than Cl^-.

B. Langevin function describes the dielectric decrement

To quantify the trends shown in Fig. 4, we describe the concentration-dependent behavior of the static permittivity $\varepsilon_R(c^S)$ by a Langevin equation:

$$\varepsilon_R(c^S) = \varepsilon_R(0) - \Delta\varepsilon\, L\left(\frac{3}{\Delta\varepsilon}\frac{\Delta P}{}\, c^S\right), \tag{13}$$

where the Langevin function $L(x) = \coth(x) - 1/x$ is employed. This formulation was initially introduced by Gavish and Promislow to describe the permittivity decrement in aqueous electrolyte solutions.[45] Its applicability has since been extended to more complex fluids, including aqueous ionic liquid mixtures, as demonstrated in our previous work.[51] We note that in ternary amino acid–salt–water systems, the Langevin parameters $\Delta\varepsilon$ and ΔP should be regarded primarily as phenomenological descriptors of the observed concentration dependence of the dielectric decrement, rather than quantities with a unique microscopic interpretation. As shown in Fig. 4, the characteristic Langevin-type response is not limited to the total permittivity decrement (bottom panels) but also holds for the individual permittivity contributions of the amino acid and water (top and middle panels, respectively). For each fit, $\varepsilon_R(0)$ is the relative permittivity at the zero-frequency limit, at zero salt concentration ($c^S = 0$) of that species. The total permittivity was evaluated with the high-frequency limit $\varepsilon_\infty(c^s)$ subtracted, which does not influence the fitting parameters ΔP and $\Delta\varepsilon$. The values of $\varepsilon_R(0)$ were calculated from the time correlation function $C(t)$ at $t = 0$. We used the

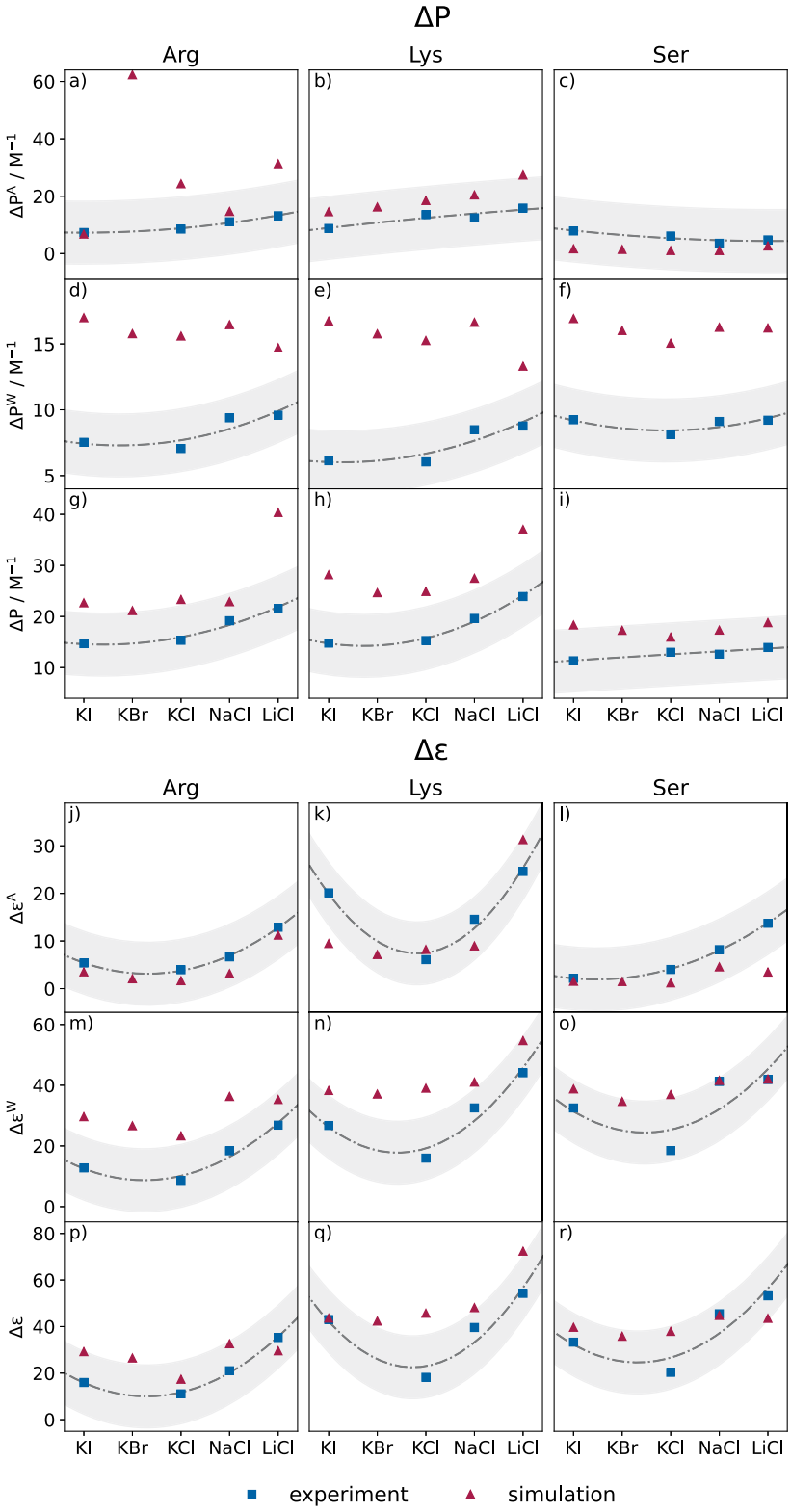

FIG. 5. Fit parameters (a)–(i) ΔP and (j)–(r) $\Delta\varepsilon$ for experiments (blue) and simulations (red). The top row is the fitting parameter of the amino acid, the middle row is of water, and the bottom row is of the whole system. The gray parabola was fitted according to experimental data and carries no physical meaning.

static permittivity $\varepsilon_R(0)$ from the binary mixtures as a constant for our fitting method to ensure comparability between different salts. Since we deal with ternary mixtures (containing the amino acid, salt, and water), the original meaning[45] of $\Delta\varepsilon$ as the difference between the dielectric constant of water and the molten salt is no longer applicable. Instead, $\Delta\varepsilon$ represents the difference between the dielectric constants at zero salt concentration, $\varepsilon_R(0)$, and at the limit of high electrolyte concentration and is derived as a fit parameter. The parameter ΔP denotes the total excess polarization of the salt.[45] It affects not only the curvature of concentration-dependent behavior at high salt concentrations but also the initial decrement, that is, $\varepsilon(c^S) = \varepsilon(0) - \Delta P \cdot c^S$ for very low concentrations c^S.

Figure 5 presents the fitted parameters ΔP and $\Delta\varepsilon$ obtained from both simulations and experiments. The salts on the x-axis are arranged from chaotropic to kosmotropic: potassium iodide represents the most chaotropic case, followed sequentially by potassium bromide and potassium chloride. Cation variations were then analyzed in order of increasing kosmotropic character, beginning with potassium, followed by sodium, and finally lithium. Across the examined salt series, KCl consistently exhibits the lowest values of both $\Delta\varepsilon$ and, in most cases, ΔP. Especially in experimental data, the parameter $\Delta\varepsilon$ [see Figs. 5(j)–5(r)], consistently follows a parabolic trend. Chaotropic anions yield larger $\Delta\varepsilon$ values compared to kosmotropic anions, indicating a stronger perturbation of the dielectric permittivity of both amino acids and water in electrolyte solutions. In contrast, for cations, the effect is reversed: kosmotropic cations exert the strongest influence on $\Delta\varepsilon$. This behavior closely parallels the established Hofmeister ordering.[7] Overall, the computational and experimental results display comparable trends across all three investigated amino acids, underscoring the robustness and transferability of the observed ordering.

The curvature parameter ΔP [see Figs. 5(a)–5(i)] exhibits considerably larger variability and is markedly more sensitive to statistical fluctuations, particularly in the dilute concentration regime, where small absolute uncertainties translate into substantial relative deviations. As a result, no systematic or statistically robust Hofmeister-type ordering can be established for ΔP based on the present data. We can see that the ΔP^W parameter is considerably lower than ΔP^A, which is reflected in the smaller curvature of ε_R^W compared to ε_R^A in Fig. 4.

Overall, the Langevin model provides an excellent empirical description of the dielectric decrement over the entire salt concentration range c^S. In addition, it fits into Debye's dielectric saturation theory:[55,56] the linear behavior at low ion concentration, due to the alignment of the water dipoles with the electric field strength of the ions, transitions into a saturation regime where the slope of the dielectric decrement vanishes with increasing salt concentration. However, a mechanistically unambiguous interpretation of the underlying parameters $\Delta\varepsilon$ and ΔP remains challenging, indicating that these fitted quantities, while quantitatively descriptive, do not directly yield conclusive insight into the molecular origin of ion-specific effects without further structural or dynamical decomposition. Nevertheless, the two parameters $\Delta\varepsilon$ and ΔP depend on the amino acid–salt combination and, therefore, are ion-specific properties. We can see that although the absolute values of $\Delta\varepsilon$ between experiments and simulations vary, the relative order is consistent. This means that the difference between the static permittivity of the binary amino acid and water solution and the theoretical minimum of permittivity in ternary solutions with different salts correlates with the order of the Hofmeister series. Kosmotropic cations with high charge density and chaotropic anions with low charge density have a greater influence on the static permittivity than chaotropic cations and kosmotropic anions. Furthermore, this parameter not only describes the total permittivity of the ternary solutions but can also be decomposed into water and amino acid contributions to the permittivity, which follow the same trend.

IV. COLLECTIVE DYNAMICS AND IMPLICATIONS FOR STRUCTURAL PROPERTIES

The influence of dissolved salts on the relaxation dynamics of water has been examined extensively and is often discussed in connection with the Hofmeister series.[57–61] Recent computational studies have emphasized the role of ions on the orientational correlations among solvent molecules, which is quantified by the Kirkwood factor g_K, and links these correlations to macroscopic dielectric responses.[22,60] In this work, we extend these concepts to more complex multicomponent systems comprising two distinct dipolar species: water and amino acids. The introduction of amino acids modifies the intrinsic hydrogen-bond network of water, generating an additional level of structural organization. Subsequent addition of salt perturbs this composite network, influencing both the long-range structuring of water and the orientational correlations of the amino acids. Our results show that several salt-induced effects observed in binary salt–water solutions persist in ternary mixtures. Moreover, specific trends can be linked to distinct contributions of the individual components, offering a more nuanced understanding of how salts modulate the collective dielectric and structural properties of such mixed systems.

A. Salt effects on collective reorientation dynamics

Apart from the dielectric decrement, the salt significantly impacts the relaxation times of the dipolar species in the ternary solutions. The relaxation times obtained from experiments and simulations are depicted in Fig. 6. The amino acid peaks consistently exhibit red shifts with increasing salt concentration, which manifests as an increase in τ^A/τ^{AA}. In contrast, the behavior of the water band shows either blue or red shifts depending on the specific combination of salt and amino acid. The relaxation times τ^A and τ^W derived from the experimental spectra (Fig. 6, bottom part of each panel) were obtained using Eq. (1). For the analysis of computational relaxation times τ^{AA} and τ^{WW} (see Fig. 6, top part of each panel), only the autocorrelation functions C^{AA} and C^{WW} from Eq. (4) were evaluated. When we analyzed the permittivity, we combined the terms of the amino acid–water and amino acid–amino acid to obtain the total contribution of the amino acid. This combination was possible, as the static permittivity can be derived directly from the simulation coordinates without any fitting procedures, and the total permittivity is simply the sum of the individual contributions. The relaxation times do not exhibit this additive behavior. Therefore, we considered only the self-terms for each molecular species (C^{AA} and C^{WW}). We employed a KWW fit, as in Eq. (8), and the relaxation times were then extracted according to Eq. (11). This approach ensures a meaningful and consistent comparison between computationally derived and experimentally measured relaxation times. While cross-term

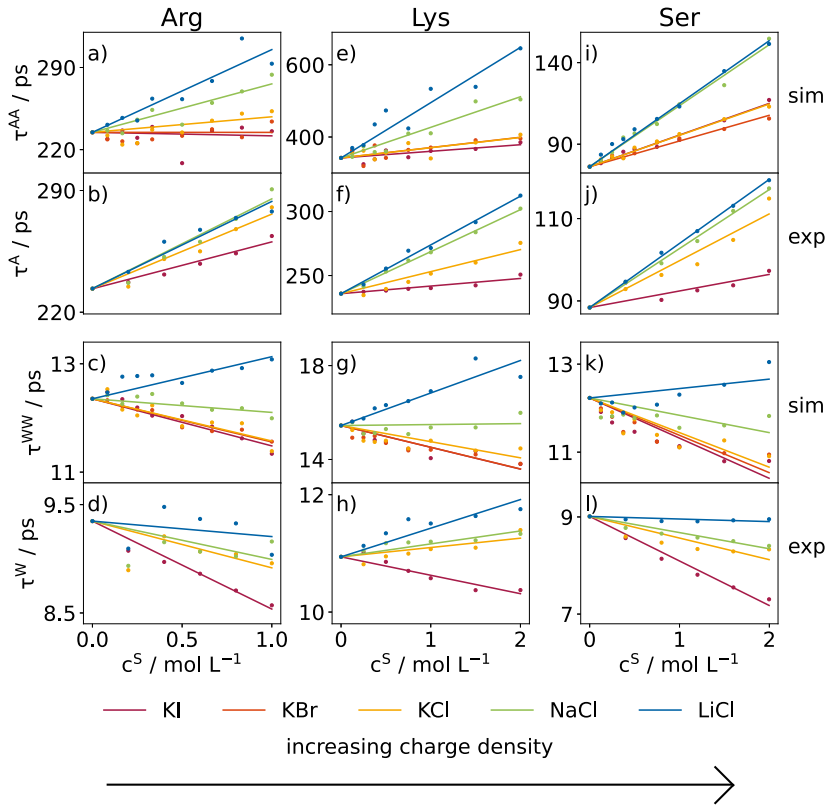

FIG. 6. Collective relaxation times of amino acids and water obtained from KWW fits and subsequently converted according to Eq. (11), where only self-terms are included in the simulations and relaxation times from experimental fit parameters. Top and bottom parts of each panel concerns the computational and experimental results, respectively: (a)–(d) of Arg, (f)–(h) of Lys, and (i)–(l) of Ser.

relaxation modes are omitted, they cannot be added to the relaxation time in a meaningful way. In contrast, including cross-correlation terms within a single KWW fit can bias the resulting relaxation times, as a single characteristic time would then be forced to represent multiple relaxation processes that occur on different time scales. This methodological distinction is crucial for water in lysine-containing mixtures, where the relaxation time associated with the cross-term is approximately an order of magnitude shorter than that of bulk-like water. This is due to the different time scales on which lysine and water relax. Usually, the cross-term of relaxation between different species lies between the peaks of each species. Lysine has the lowest relaxation time of all tested amino acids; concomitantly, the lysine–water cross-correlation relaxation time is the slowest. Taking the average of the self- and cross-correlation relaxation times would skew the perceived relaxation time toward lower time scales. Furthermore, this averaged relaxation time would not reflect the peak maxima in the spectra. As the experimental fit was derived from a two-peak fit model, we only get two relaxation times, whereas from a computational standpoint we have three (amino acid–water and water–amino acid correlation peaks should ideally have perfect overlap). There is no meaningful way to combine the τ value of the cross-terms with the self-terms. As we only have two peaks in the experiments, we chose the two self-terms to compare the computational results with the experimental results. Moreover, this approach facilitates direct comparison with the single-particle dipole relaxation times derived from the single-particle dipole autocorrelation function (see Sec. SV in the supplementary material), which is essential for interpreting the correlation between the microscopic structure and dynamical heterogeneity of the liquid.

The analysis of the fitted parameters shows that the relaxation times of the amino acids increase systematically with rising salt concentration, as illustrated in the top row of Fig. 6. This trend agrees with earlier reports,[14,62] which relate the effect to a salt-induced increase in the effective viscosity of the solution. The behavior of water in the ternary solutions is markedly different: in all binary systems, the relaxation time of water exceeds that of bulk water, with values of 9.01–10.9 ps in the experiments and 12.2–15.4 ps in the simulations, depending on the amino acid. Among the investigated solutes, Ser induces the smallest increase, whereas Lys produces the most pronounced slowdown. For comparison, previously reported bulk values amount to 8.38 ps[63] in experiments and 8.5–11.1 ps[64] for SPC/E water. The elevated relaxation times in the binary amino acid solutions can be attributed to the retarded dynamics of hydration water near the solutes, which effectively increases the local viscosity. Upon addition of salt, the relaxation time of water may either increase or decrease, depending on the specific amino acid–salt combination, and minor discrepancies between experiment and simulation are observed. Reductions in the relaxation time are commonly associated with a weakening of the hydrogen bond network,[63,65] the perturbation of collective water dynamics, and modifications of dipolar correlations induced by the ions.[66,67]

As discussed by Feldman and Ben Ishai,[68] the addition of ions to aqueous solutions typically induces a blue shift of the water

relaxation peak, whereas the presence of polar solutes leads to a red shift. Consequently, the relaxation times of water in binary amino acid–water mixtures exceed those of pure water. Upon introducing salts into these mixtures, however, the relaxation times decrease for certain ions, as shown in the bottom row of Fig. 6. For molecular solutes such as amino acids, which possess both ionic and dipolar character, the dependence of relaxation dynamics on concentration is intrinsically complex and does not follow a simple monotonic relationship.[68] The addition of salt to such systems triggers several competing mechanisms: some processes promote slower dynamics, whereas others accelerate the reorientation of water in the ternary mixtures. Despite this interplay, a clear trend emerges across all studied systems. Ions with higher charge densities systematically produce larger increases in the water relaxation time as salt concentration rises. To quantify this effect, we applied a linear model in which we kept the relaxation time of the constituent in the corresponding binary mixture constant to allow for comparability across systems. The resulting fits show that ions with higher charge density yield higher slopes. This indicates that there is a specific ion effect on relaxation times. Kosmotropic ions lead to higher relaxation times of the amino acid and the water relaxation. Chaotropic ions give rise to lower relaxation times of amino acids and can even lead to relaxation times of water that are lower than in binary water–amino acid mixtures.

B. Single-particle rotation and collective dielectric response

We evaluated the single-particle relaxation times of both amino acids and water from the MD trajectories; the results are presented in Fig. S10 in the supplementary material. The single-particle relaxation times increase in all cases, for both amino acid and water relaxation modes. This indicates that the relaxation of individual molecules is decelerated by ions in all cases. The higher the charge densities of the ions, the slower the molecular relaxation times. The relationship between single-particle relaxation times τ_{mol} and collective relaxation times τ can provide information about the structure of the liquid system. The structural organization of the liquid and its collective dynamical response are inherently linked through the Kirkwood factor g_K, shown in Fig. 7. From a dynamical perspective, g_K represents the ratio of the collective relaxation time τ to the single-molecule relaxation time τ_{mol}, known as the Kivelson–Madden relationship in Eq. (14):[69–71]

$$g_K = \frac{\tau}{\tau_{mol}}, \tag{14}$$

$$g_K = \frac{\langle M_D^2 \rangle}{N\langle \mu^2 \rangle}. \tag{15}$$

The second equation, Eq. (15), provides a static interpretation, relating the collective dipole moment M_D to the single-molecule dipole moment μ, where N denotes the number of molecules of the species under consideration. Thus, $\langle M_D^2 \rangle / N$ can be regarded as an effective dipole moment μ_{eff}^2. A decrease in τ accompanied by an increase in τ_{mol} therefore leads to a pronounced reduction in g_K, reflecting a decrease in parallel or an increase in antiparallel correlations within the system. As shown in Fig. 7, Kirkwood factors below unity indicate predominantly antiparallel dipole arrangements.[72] Such

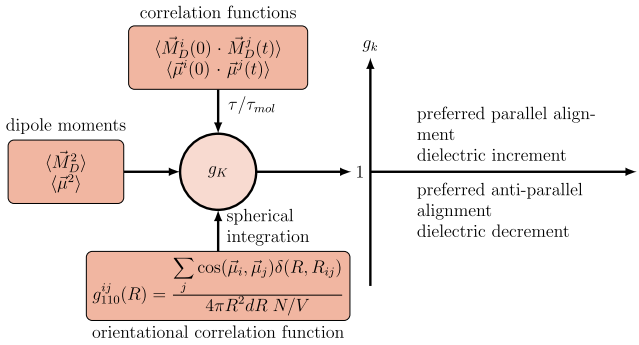

FIG. 7. Kirkwood g_K factor describes the correlation between collective and single-particle phenomena, derived from both structure and dynamics.

configurations relax more rapidly than parallel dipole alignments, as the collective dipole moment relaxation is heavily influenced by individual molecular reorientation.[72] Honegger and Steinhauser describe that two molecules possessing the same single-particle relaxation time can exhibit different collective relaxation behaviors depending on their relative orientation.[72] When dipoles are already positively correlated, the absolute value of the collective dipole moment is large, but the angle of rotation of the collective dipole moment is comparatively low.[72] This behavior manifests as high permittivities and slow relaxation times. When two dipole moments are already antiparallel, the value of the collective dipole moment is small.[72] However, small rotations of the molecules can effectively flip the collective dipole moment by up to 180°.[72]

This implies that the reduction in τ^W and τ^{WW} in Figs. 6(c), 6(d), 6(g), 6(h), 6(k), and 6(l), together with the accompanying decrease in permittivity [see Figs. 4(c), 4(d), 4(i), 4(j), 4(o), and 4(p)], can arise from a smaller number of water molecules effectively contributing to the collective fluctuations of the macroscopic polarization. In such situations, the reorientation of the remaining contributing molecules has a disproportionately larger impact on the dielectric response than in systems where a larger fraction of water participates. Consistent with this interpretation, the collective relaxation times of water approach the corresponding single-molecule relaxation times as the salt concentration increases. In binary amino acid–water mixtures, τ_{mol}^W is significantly lower than τ^{WW}. With increasing salt concentration, these two values become closer to each other. An increase in single-particle relaxation times τ_{mol} combined with a decrease in collective relaxation times τ can be traced to disruptions in the microscopic organization of the liquid. In particular, the behavior is consistent with increasing dipole–dipole anti-correlation or decreasing dipole–dipole correlation.

The behavior observed for the amino acids is different: in most systems, the collective relaxation times closely match the molecular relaxation times. This indicates that there is no significant amino acid–amino acid correlation. A notable exception occurs in mixtures containing lithium ions, where the molecular relaxation times are significantly longer than the collective ones. Strong ion–amino acid coordination restricts individual molecular reorientation, thereby increasing the single-particle dipole relaxation times. The shorter collective relaxation times, in turn, can be explained by antiparallel dipole alignment within these coordinated structures as depicted in Fig. 8(d). Because these associated dipole moments

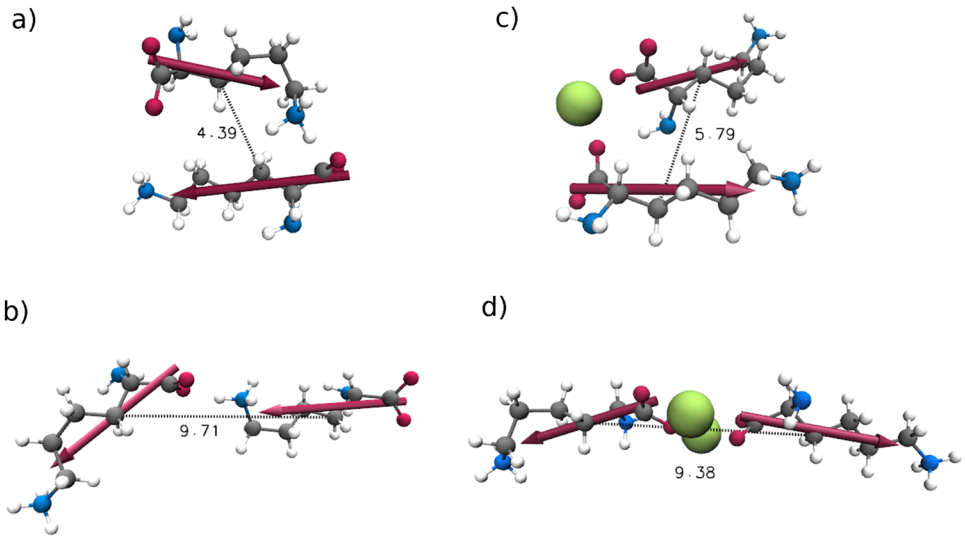

FIG. 8. Snapshots from the simulations of parallel and antiparallel dipole alignments of lysine molecules. (a) and (b) show the conformations found in binary solutions and all electrolyte solutions other than high concentrations of LiCl and (c) and (d) show how lithium ions flip the dipole–dipole orientation of the amino acid–amino acid conformations. The red arrows are the dipole moments, and the distances are distances from β-carbon to β-carbon.

largely cancel their contribution to the permittivity, these slowly reorienting molecules do not contribute to the collective dielectric relaxation. In contrast, amino acids in solutions with less strongly coordinating salts exhibit collective relaxation times comparable to the corresponding molecular relaxation times, indicating that the collective amino acid relaxation in these systems is primarily governed by the rotational dynamics of individual molecules. In the absence of nearby ions, amino acids favor a parallel, head–tail alignment, as illustrated in Fig. 8(b), since this geometry maximizes the dipole–dipole attraction between neighboring dipolar species. The radial distribution function g_{000} and the dipole–dipole orientational radial distribution g_{110} can be used to assess how molecules are positioned. For more information on these functions, see supplementary material, Sec. SVI. The amino acid–amino acid $g_{000}(r)$ and $g_{110}(r)$ (see supplementary material, Figs. S11–S16 first column) functions both have a maximum at the distance where tail-to-tail ordering occurs, indicating that the local density at that distance is enriched and that they are parallel aligned, as in Fig. 8(b). Another possible conformation is the side-to-side ordering of amino acids, as depicted in Fig. 8(a). This conformation is, however, depleted for arginine in the $g_{000}(r)$ function (see supplementary material, Figs. S11 and S14). The coordination of lithium flips the dipole–dipole orientation. The two initial extrema in the $g_{110}(r)$ function for arginine and lysine (see supplementary material, Figs. S14 and S15) flip, meaning the minimum in the $g_{110}(r)$, which is the antiparallel orientation at close distances like Fig. 8(a) becomes a maximum due to coordination of two or more amino acids to one lithium ion, like in Fig. 8(c). The head-to-tail conformation in Fig. 8(b) which is observable as the maximum in the $g_{110}(r)$ function, becomes a head-to-head conformation as shown in Fig. 8(b). All other salts have single-particle relaxation times that are similar to collective relaxation times. Under these conditions, the rotational motion of the individual molecular amino acid dipoles contributes directly to the overall polarization of the system and is not impeded by additional coordinating interactions.

The single-particle relaxation times increase for all amino acid and water contributions with increasing salt concentration for all salts. Salts with higher charge density lead to higher single-particle relaxation times. The relationship between τ_{mol} and τ can provide information on the structure of the liquid. Amino acid contributions show that τ_{mol} and τ are similar in all ternary mixtures except for systems containing Li^+. This indicates that there is no strong amino acid–amino acid dipole–dipole correlation. The contrasting trends in the dielectric relaxation behavior of water—i.e., the increase in single-particle relaxation times with simultaneously decreasing collective relaxation times—are consistent with increasingly antiparallel alignment of water molecules in the solution. Therefore, the decrease in collective relaxation time can indicate less parallel alignment of water–water dipole–dipole correlations.

V. STRUCTURAL ANALYSIS

A. Structural analysis of dipole correlations via $g_{110}(r)$ and the Kirkwood factor

While the Kivelson–Madden relationship in Eq. (14) offers valuable conceptual insight, it exhibits two principal limitations. First, it requires an additional proportionality constant [see supplementary material, Eq. (S10)] that is frequently omitted in practical applications, thereby reducing its quantitative reliability.[64] Second, it does not adequately account for cross-correlations in multicomponent systems, where dipolar interactions between distinct species play a significant role.[73] To overcome these limitations, the dipole–dipole orientational radial distribution function[37,74,75] $g_{110}(r)$ can be employed to characterize the relative orientations of dipoles belonging to different molecular species. The corresponding $g_{110}(r)$ functions for the systems studied here are shown in Figs. S14–S16 of the supplementary material. Integration of $g_{110}(r)$ over spherical shells yields[73,76] the spatially resolved Kirkwood factor,

$$g_K(r) = 1 + \frac{N}{V}\int_0^r 4\pi R^2\, g_{110}(R)\, dR, \tag{16}$$

which provides a more complete description of dipolar correlations by explicitly incorporating both intra- (ii) and interspecies (ij)

orientational contributions. One limitation of evaluating g_K via Eq. (16) is its sensitivity to statistical noise at larger intermolecular distances. Numerical noise in this long-range region strongly affects the integral, thereby distorting the resulting g_K values. In our simulations, we observe that all $g_{110}(R)$ functions decay toward zero at shorter distances for systems with higher salt concentrations than for systems with lower ionic strength. None of the binary systems converge to zero, even at large distances. Consequently, when g_K is computed from Eq. (16), an apparent increase may emerge at low salt concentrations before a decrease sets in at higher concentrations, which might be due to limited simulation box lengths. When g_{110}^{AW} does not level off to zero at half the box length, the spatially resolved g_K^{AW} does not plateau, which means the value is not converged and, therefore, not assured. We conducted additional simulations with increased box sizes; however, we were unable to completely eliminate this effect. We discuss the size effect and the concentration dependence on the plateauing behavior of the spatially resolved g_K^{AW} function in greater detail in the supplementary material, Sec. SVIII.

Considering that the amino acid relaxation peak consists of two contributions ($\varepsilon_R^A = \varepsilon_R^{AA} + \varepsilon_R^{AW}$), we can now take a closer look at the contributions of amino acid–water relaxations that manifest in ε_R^{AW} and amino acid–amino acid relaxation that manifests in ε_R^{AA}, and how they relate to the collective structure. Figure 9 displays how ε_R^{AA}, g_K^{AA}, ε_R^{AW}, and g_K^{AW} behave in the different systems. Figures 9(a), 9(e), and 9(i) display the Kirkwood factors g_K for all amino acid–amino acid pairs obtained from $g_{110}(r)$, where the upper integration limit in Eq. (16) corresponds to half of the length of the simulation box. Except for LiCl, the addition of salt has no significant influence on g_K^{AA}. In all other systems, the Kirkwood factor remains close to unity, indicating an essentially random orientational distribution of amino acids in solution. This observation is consistent with the static dielectric permittivity in Figs. 9(b), 9(f), and 9(j), which is constant in all systems except for solutions containing LiCl. Thus, changes in amino acid–amino acid orientations are not responsible for the dielectric decrement associated with the amino acid relaxation peak.

Lithium chloride represents a clear outlier due to its strong coordination with the amino acids. This interaction promotes the formation of amino acid dimers or even larger aggregates, leading to a reduction in g_K and visible peak inversions in the Arg–Arg and Lys–Lys orientational correlations in the $g_{110}(r)$ functions (see Figs. S14 and S15 of the supplementary material). These structural motifs induce pronounced depolarization effects in ε_R^{AA}, a mechanism reminiscent of the frequently reported salting-in effect.[77,78] In our trajectories, we observe multiple lithium ions coordinated simultaneously to several amino acids, enforcing antiparallel dipole orientations within these clusters as depicted in Fig. 8(d). While other cations do not promote such aggregation, lithium uniquely alters the structural alignment between amino acid molecules, thereby influencing their collective dielectric response.

There is an apparent discrepancy between the constant g_K^{AW} and ε_R^{AW} in Fig. 9. The g_K^{AA} values for all K^+-containing arginine solutions appear nearly constant, which is consistent with our assessment that

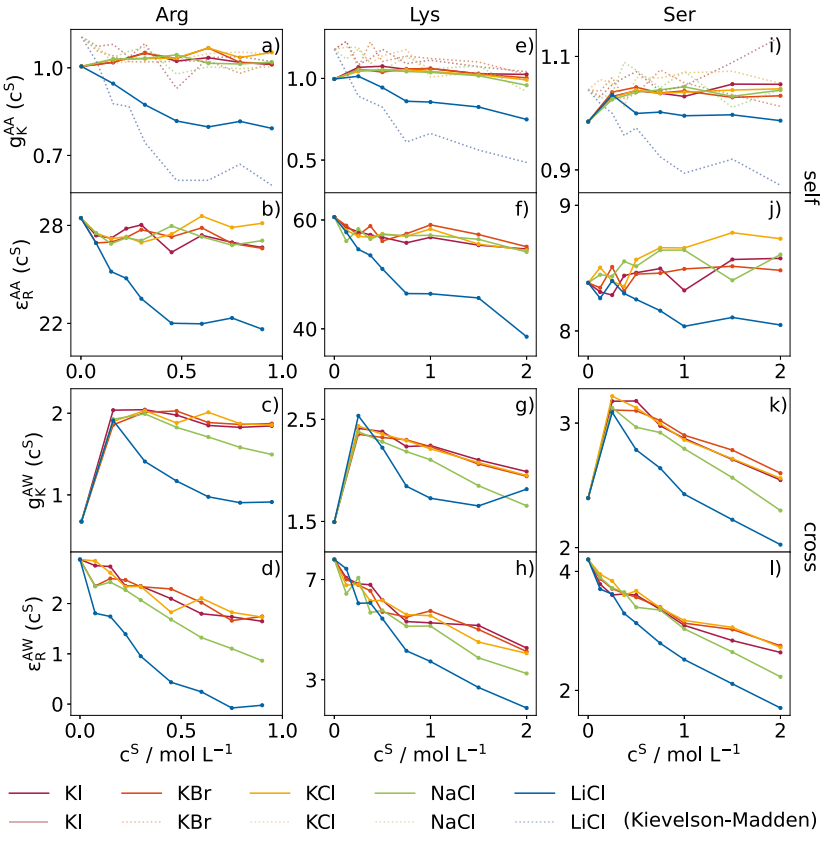

FIG. 9. Kirkwood g-factor g_K and decomposed ε_R of all amino acids and all contributions. The top panels show the self-terms of amino acid–amino acid (AA) correlations and the bottom panels show the amino acid–water (AW) correlations of arginine (left), lysine (middle), and serine (right). The structure factor of AA was calculated by Eq. (14) (dotted lines) and Eq. (16) (solid lines) for comparison. As the Kivelson–Madden relationship cannot be applied to mixed species, they were only evaluated according to Eq. (16) (solid lines). The contributions ε_R^{AW} and ε_R^{AA} to ε_R were calculated according to Eq. (4) where $j \neq i$ and $j = i$, respectively.

ε_R^{AA} is constant. However, all g_K^{AW} of K^+-salt systems are also nearly constant in arginine systems, which does not align with the pronounced variations observed in the ε_R^{AW} contributions. Considering that ε_R^A decreases, the decrease must either be from changes in amino acid–amino acid or amino acid–water correlations. In theory g_K^{AW} and ε_R^{AW} should resemble the same trend, as ε_R can be calculated from $\vec{M}_D^2$, see Fig. 7, which we used to calculate ε_R, see Eq. (4). This discrepancy might be due to uncertainties in the g_{110} functions and subsequent integration errors. The higher the salt concentration, the faster the g_{110} function converges to zero. As the systems containing arginine have lower salt concentrations, convergence is not necessarily achieved. Section SVIII in the supplementary material discusses the convergence in greater detail. The top panels of Fig. 9 demonstrate that the Kivelson–Madden relationship captures changes in the permittivity more faithfully than the g_K obtained from the $g_{110}(r)$ function. However, because cross-terms cannot be extracted from the Kivelson–Madden expression, it remains unclear whether this discrepancy arises from integration-related uncertainties in Eq. (16) or from the possibility that potassium salts do not substantially modify the long-range orientational structure of Arg relative to water.

Overall, the decrease of ε_R^A can be attributed to a decrease in g_K^{AW}. The amino acid–amino acid correlations are not affected by the addition of salt, except for LiCl. That means that the changes in the amino acid peak are dominated by amino acid–water correlations.

B. Long-range interactions of amino acid–water dipolar cross-correlations

Even though the amino acid–amino acid (AA) orientational structure remains largely unaffected by the addition of salt, a pronounced dielectric decrement is observed in Figs. 4(a), 4(b), 4(g), 4(h), 4(m), and 4(n). Our analysis shows a systematic reduction in the Kirkwood factor g_K for all amino acids and salts when amino acid–water (AW) correlations are considered, as shown in Figs. 9(c), 9(g), and 9(k). This decrease originates from the strong local ion fields, which disrupt dipolar ordering well beyond the first solvation shell. We found that the decrease in g_K^{AW} is mainly caused by long-range restructuring beyond the first two solvation shells, which can be observed as the second minimum in the g_{000} functions. A reduction in g_K reflects an increasing tendency toward antiparallel alignment between water and amino acid dipoles, which in turn causes a substantial decrease in the cross-term ε_R^{AW} in Figs. 9(d), 9(h), and 9(i).

A schematic representation of the dominant dipole–dipole interactions between the amino acid and surrounding water molecules is provided in Fig. 10. Within the first solvation shell, the correlation function $g_{110}(r)$ assumes negative values at very short distances, reflecting the preferred side-by-side orientation of the amino acid and water dipoles [see Fig. 10(b)]. The pronounced maximum at ~4 to 5 Å arises from head–tail configurations in which the dipoles are aligned in parallel (supplementary material Figs. S14–S16 show the g_{110} functions for all amino acids and salts; the AW correlations are the middle columns). Owing to the long-range nature of dipole–dipole interactions, water molecules at distances beyond 10 Å also tend toward parallel alignment. However, these effects are barely visible in the g_{110} function as it converges to zero at these distances. At elevated salt concentrations, shown in Fig. 10(a),

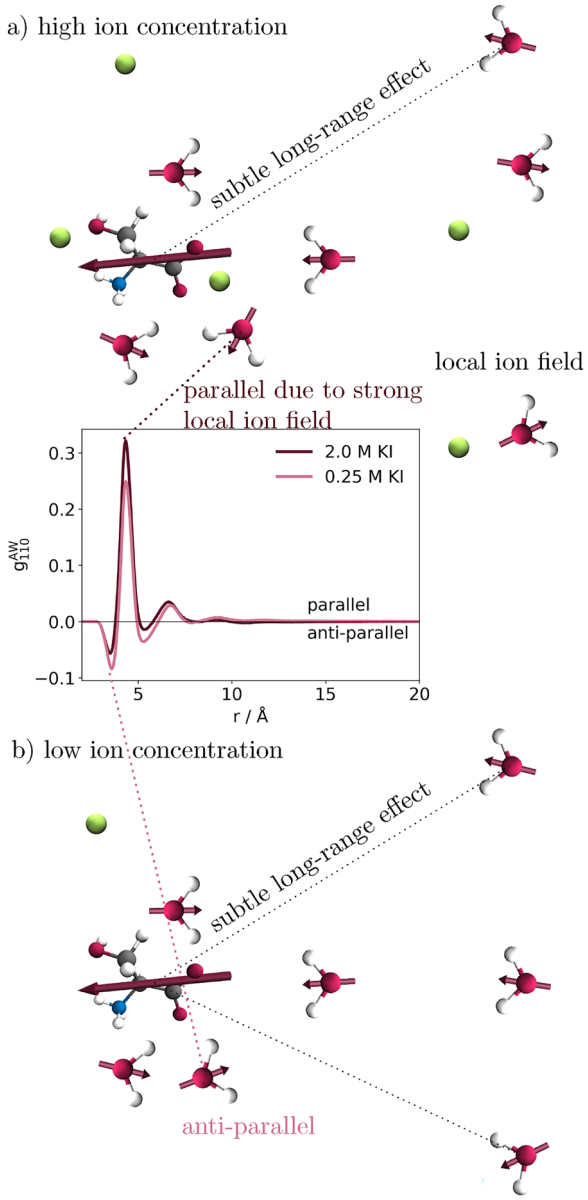

FIG. 10. Schematic representation of the Ser-water orientation based on $g_{110}(r)$ at low (a) and high (b) salt concentration. The local ion field may overlay the subtle long-range dipole–dipole interaction between the amino acid and water. The g_{110} function of solutions with low concentration (0.25 mol L^{-1}) and high concentration (2.0 mol L^{-1}) of KI are shown to demonstrate the effects on the dipole–dipole orientation of water around amino acids.

the water dipole orientations in close proximity to the amino acid are less antiparallel at the first minimum and more parallel at the first maximum compared to low salt concentrations. This is due to strong local ion fields and the parallel alignment of water molecules when water and amino acids are affected by the same ion field. The initial two peaks of the g_{110} function would indicate more parallel alignment and, therefore, a higher g_K. However, the long-range

effects—i.e., alignments of dipole moments beyond the first two solvation shells—dominate the overall g_K, which we can see as g_K^{AW} decreases with increasing salt concentrations in Fig. 9. Local ion fields generated by the ions dominate the orientational ordering of the water dipoles and strongly counteract the long-range orientational influence of the amino acid. In extreme cases, such as Arg in LiCl solutions, the permittivity from cross-correlations ε_R^{AW} approaches zero at high salt concentrations (0.75 mol L^{-1}). The behavior of the g_{110}^{AW} functions (see supplementary material S14–S16 middle columns) can be generalized. We can see that the two initial peaks in these functions are less negative or more positive, respectively, at high salt concentration. This indicates that there is more parallel alignment of water in proximity to amino acid molecules at high salt concentration. As the overall g_K decreases with increasing salt concentration, the total parallel alignment, however, must decrease with increasing salt concentration. This decrease in parallel alignment must, therefore, come from subtle long-range effects. This behavior indicates that the dielectric decrement associated with the amino acid peak is largely governed by ion-induced alterations in the long-range water–amino acid dipole structure, rather than by neighboring amino acid–water interactions.

This behavior resembles the findings of Zhang *et al.*[22] for aqueous salt solutions. They reported that, although the structure of bulk water remains largely unaffected by the addition of salt, the cross-correlation between bulk water and water in the solvation shell exhibits a characteristic arc-like dependence on salt concentration. While we did not explicitly separate bulk and hydration-shell water in our analysis, we observe analogous trends in both the AA and AW correlations. Long-range correlations of amino acid and water influence the overall ε_R. As depicted in Fig. 10(a), the orientation of water molecules that are part of an ion shell is influenced by local ion fields. The reorientation of water and amino acid molecules, which are affected by different ionic fields, can lead to long-range anticorrelations. The local ion fields disrupt the long-range orientation of dipole moments beyond the first solvation shell. This can also be observed in the g_{110} functions, which approach zero more quickly in solutions with higher salt concentrations. However, this effect is very subtle, whereas the change in the structure of the first solvation shells can be observed from the g_{110} functions. In contrast, AA correlations remain largely unchanged across all salts and concentrations [see Figs. 9(a), 9(e), and 9(i)], except in the presence of Li^+ ions. Lithium induces enhanced amino acid coordination, resulting in a nonlinear reduction of the AA contributions (blue curve). This effect is due to the direct influence of lithium on the amino acid–amino acid orientations [see Figs. 8(c) and 8(d)]. For all other ions, the AA dipole–dipole correlations remain essentially unaffected, mirroring the invariant bulk water–bulk water correlations described by others.[22,60] While amino acids are coordinated to an ion, they are rarely coordinated to the same ion; therefore, they move independently.

Given that amino acids are known to be strongly hydrated,[43] the addition of salts could modify the size and/or structure of their hydration shells.[17,18] The first minimum in $g_{110}^{AW}(r)$ for amino acids and water (see supplementary material, Figs. S14–S16, middle panels) becomes progressively shallower with increasing salt concentration, which, in isolation, would lead to an increase in g_K. Similarly, the subsequent maximum grows in intensity and would likewise contribute positively to g_K. However, depolarization is not a purely local phenomenon. The features discussed above occur at short intermolecular distances, where the volume of the corresponding spherical shells is small, and thus their contributions to the integral in Eq. (16) are minor. As a result, the dominant effect is a net decrease in g_K with rising salt concentration, demonstrating that ion-induced perturbations of dipolar order extend well beyond the first solvation shell.

VI. CONCLUSION

Our combined experimental and computational analysis demonstrates that the dielectric response of aqueous amino acid–salt solutions is governed by robust and systematic ion-specific effects. Across all systems, the static permittivity decreases monotonically with increasing salt concentration and is accurately described by a phenomenological Langevin-type functional form for both the total permittivity and the decomposed contributions of water and amino acids. The magnitude of this dielectric decrement follows a clear Hofmeister-type ordering: cations with high charge density, most notably Li^+, induce the strongest reduction in permittivity. Anionic effects are generally weaker and more variable, but they also follow established chaotropic/kosmotropic trends; anions with lower charge density, such as I^-, invoke greater changes. In this sense, the observed trends parallel classical salting-in and salting-out behavior, where ions of different hydration strengths modulate the effective interactions and dynamic response of solutes. Figure 11, row 4, shows that the static permittivity ε_R decreases for all salts, with the smallest decrease observed for KCl and progressively larger decreases for cations with higher charge density and anions with lower charge density.

MD simulations reveal that the decrease in permittivity originates not from changes in the permanent dipole moments of the amino acids, but rather from ion-induced restructuring of dipolar correlations. Strongly kosmotropic cations preferentially coordinate to the carboxylate groups and, in extreme cases, promote the

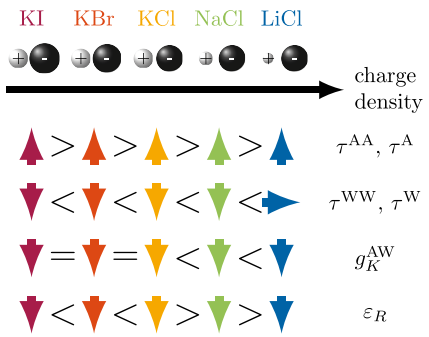

FIG. 11. Ranking of the dielectric properties in the Ser solutions of this study as a function of the added alkali halide salt. The ionic charge density increases systematically from KI to LiCl. The symbols >, =, and < denote whether the respective property decreases, remains unchanged, or increases with increasing ionic charge density. Colored arrows indicate the variation of each property with increasing salt concentration, where upward arrows represent an increase and downward arrows a decrease. The arrow colors distinguish the different salt species. The indices AA and WW indicate the collective relaxation times of the computational correlation functions of the amino acid and water. The indices A and W are the respective indices for the experimental data.

formation of amino acid dimers or small aggregates with antiparallel dipole alignment. This results in substantial depolarization of the amino acid contribution to the permittivity, an effect consistent with ion-induced modulation of solute–solute interactions seen in salting-in/out phenomena. In contrast, amino acid–amino acid orientational correlations remain largely unaffected by all other salts, underscoring that the dominant structural perturbations arise from modifications of amino acid–water and water–water dipolar correlations rather than direct changes in amino acid packing.

The relaxation dynamics similarly reflect ion-specific behavior as sketched in Fig. 11. The relaxation times of the amino acid modes increase with rising salt concentration (upward arrows in the first row) and correlate with ionic charge density, with LiCl again producing the most pronounced slowdown. The water relaxation dynamics exhibit a more complex interplay of effects: although the single-particle reorientation of water universally slows down upon salt addition, the collective water relaxation time may decrease for ions of lower charge density (second row in Fig. 11). This divergence between single-particle and collective dynamics reflects the disruption of long-range dipolar networks and an enhanced antiparallel alignment that reduces the number of molecules contributing cooperatively to the collective mode.

In this context, it is worthwhile to mention that at higher electrolyte concentrations, or for ion species with a stronger propensity for ion–ion association, ion pairing and the formation of ionic aggregates may become increasingly relevant and can modify the dielectric response. In dielectric spectroscopy, such effects may manifest as additional low-frequency relaxation processes and deviations from simple Debye or Cole–Cole behavior. In this regime, the dielectric decrement and relaxation dynamics are no longer governed solely by solvent-mediated dipolar correlations, and explicit ion–ion correlations would need to be considered. The present framework, therefore, applies most directly to the concentration ranges explored in this work, where no additional relaxation processes are observed within the present experimental window. From a computational point of view, ϑ, discussed in the supplementary material in Sec. SII, cannot be neglected at high concentration regimes of electrolytic solutions.

Altogether, these results show that specific ion effects in electrolyte–amino acid mixtures manifest primarily through the modulation of long-range orientational correlations rather than through local changes in hydration structure alone. This perspective is consistent with broader frameworks used to rationalize salting-in and salting-out behavior, suggesting that even simple amino acid solutions capture essential features of Hofmeister-type specificity. While amino acids constitute only minimalistic models of biomolecular building blocks, the trends identified here may provide microscopic insight into how ions modulate interactions in more complex systems. Further work will be required to assess how these mechanisms extend to peptides and proteins, where additional structural and dynamical factors come into play.

SUPPLEMENTARY MATERIAL

The supplementary material contains supporting experimental dielectric spectra and analysis (pH measurements, concentration dependence, spectral decomposition, Cole–Cole parameters, and conductivity), as well as dielectric spectra of ternary amino acid–salt solutions. Additional simulation methodology and results are included, comprising single-particle relaxation times, molecular radial and orientational correlation functions, water-structure metrics, force-field parameters, and finite-size/convergence assessments.

ACKNOWLEDGMENTS

The authors would like to thank Othmar Steinhauser for helpful discussions. We also thank Martina Knecht for support with sample preparation, pH measurements, and dielectric spectroscopy experiments. Vasileios Balos acknowledges financial support from the Comunidad de Madrid under the project "Cesar Nombela" No. 2023-T1/TEC-29119, and the "Programa de Actividades de I+D entre Grupos de Investigación de la Comunidad de Madrid en Tecnologías 2024" FotoArt5.0-CM—No. TEC-2024/TEC-308.

AUTHOR DECLARATIONS

Conflict of Interest

The authors have no conflicts to disclose.

Author Contributions

Marion Sappl: Data curation (equal); Formal analysis (lead); Investigation (lead); Methodology (lead); Validation (equal); Visualization (lead); Writing – original draft (lead); Writing – review & editing (equal). **Christian Fellinger**: Formal analysis (supporting); Investigation (supporting); Methodology (supporting); Validation (supporting); Writing – review & editing (supporting). **Amala Elizabeth**: Investigation (supporting). **Dimitra Kanta**: Investigation (supporting). **Leon Prädel**: Investigation (supporting). **Johannes Hunger**: Conceptualization (lead); Formal analysis (equal); Methodology (lead); Resources (supporting); Supervision (lead); Validation (equal); Writing – review & editing (lead). **Christian Schröder**: Conceptualization (lead); Formal analysis (equal); Methodology (equal); Supervision (lead); Validation (equal); Writing – original draft (supporting); Writing – review & editing (lead). **Vasileios Balos**: Conceptualization (lead); Formal analysis (equal); Funding acquisition (lead); Investigation (lead); Methodology (lead); Supervision (lead); Validation (equal); Visualization (equal); Writing – original draft (supporting); Writing – review & editing (lead).

DATA AVAILABILITY

The experimental and computational data that support the findings of this study are available from the corresponding authors upon reasonable request.

REFERENCES

[1] P. Lo Nostro and B. W. Ninham, Chem. Rev. **112**, 2286 (2012).
[2] Y. Zhang and P. S. Cremer, Curr. Opin. Chem. Biol. **10**, 658 (2006).
[3] Y. Zhang, S. Furyk, D. E. Bergbreiter, and P. S. Cremer, J. Am. Chem. Soc. **127**, 14505 (2005).

[4]Y. Zhang and P. S. Cremer, Annu. Rev. Phys. Chem. **61**, 63 (2010).
[5]A. Salis and B. W. Ninham, Chem. Soc. Rev. **43**, 7358 (2014).
[6]H. I. Okur, J. Hladílková, K. B. Rembert, Y. Cho, J. Heyda, J. Dzubiella, P. S. Cremer, and P. Jungwirth, J. Phys. Chem. B **121**, 1997 (2017).
[7]K. P. Gregory, G. R. Elliott, H. Robertson, A. Kumar, E. J. Wanless, G. B. Webber, V. S. J. Craig, G. G. Andersson, and A. J. Page, Phys. Chem. Chem. Phys. **24**, 12682 (2022).
[8]F. Hofmeister, Arch. Exp. Pathol. Pharmakol. **24**, 247 (1888).
[9]N. Schwierz, D. Horinek, and R. R. Netz, Langmuir **26**, 7370 (2010).
[10]N. Schwierz, D. Horinek, U. Sivan, and R. R. Netz, Curr. Opin. Colloid Interface Sci. **23**, 10 (2016).
[11]K. D. Collins, G. W. Neilson, and J. E. Enderby, Biophys. Chem. **128**, 95 (2007).
[12]M. Kowacz, A. Mukhopadhyay, A. L. Carvalho, J. M. S. S. Esperança, M. J. Romão, and L. P. N. Rebelo, Cryst. Eng. Commun. **14**, 4912 (2012).
[13]A. Szabadi, R. Klausser, O. Spadiut, and C. Schröder, Liquids **4**, 1 (2024).
[14]V. Balos, M. Bonn, and J. Hunger, Phys. Chem. Chem. Phys. **19**, 9724 (2017).
[15]V. Balos, B. Marekha, C. Malm, M. Wagner, Y. Nagata, M. Bonn, and J. Hunger, Angew. Chem., Int. Ed. **58**, 332 (2019).
[16]E. A. Algaer and N. F. A. Van Der Vegt, J. Phys. Chem. B **115**, 13781 (2011).
[17]K. D. Collins, Methods **34**, 300 (2004).
[18]V. Balos, N. K. Kaliannan, H. Elgabarty, M. Wolf, T. D. Kühne, and M. Sajadi, Nat. Chem. **14**, 1031 (2022).
[19]M. Aliyeva, P. Brandão, J. A. P. Coutinho, O. Ferreira, and S. P. Pinho, J. Solution Chem. **53**, 527 (2024).
[20]L. I. N. Tomé, M. Jorge, J. R. B. Gomes, and J. A. P. Coutinho, J. Phys. Chem. B **114**, 16450 (2010).
[21]J. Heyda, T. Hrobárik, and P. Jungwirth, J. Phys. Chem. A **113**, 1969 (2009).
[22]C. Zhang, S. Yue, A. Z. Panagiotopoulos, M. L. Klein, and X. Wu, Phys. Rev. Lett. **131**, 076801 (2023).
[23]P. Eastman, R. Galvelis, R. P. Peláez, C. R. A. Abreu, S. E. Farr, E. Gallicchio, A. Gorenko, M. M. Henry, F. Hu, J. Huang, A. Krämer, J. Michel, J. A. Mitchell, V. S. Pande, J. P. Rodrigues, J. Rodriguez-Guerra, A. C. Simmonett, S. Singh, J. Swails, P. Turner, Y. Wang, I. Zhang, J. D. Chodera, G. De Fabritiis, and T. E. Markland, J. Phys. Chem. B **128**, 109 (2024).
[24]J. A. Maier, C. Martinez, K. Kasavajhala, L. Wickstrom, K. E. Hauser, and C. Simmerling, J. Chem. Theory Comput. **11**, 3696 (2015).
[25]A. Barth, Prog. Biophys. Mol. Biol. **74**, 141 (2000).
[26]J. Janin, S. Wodak, M. Levitt, and B. Maigret, J. Mol. Biol. **125**, 357 (1978).
[27]W. M. Haynes, *CRC Handbook of Chemistry and Physics*, 95th ed. (CRC Press, London, New York, 2014).
[28]V. Balos, H. Kim, M. Bonn, and J. Hunger, Angew. Chem., Int. Ed. **55**, 8125 (2016).
[29]H. Geraili Daronkola and A. Vila Verde, Biophys. J. **120**, 2746 (2021).
[30]A. E. Kremer and F. Schönals, *Broadband Dielectric Spectroscopy* (Springer, 2003).
[31]M. David, Y. Feldman, and P. Ben Ishai, in *Non-Destructive Material Characterization Methods*, edited by A. Otsuki, S. Jose, M. Mohan, and S. Thomas (Elsevier, 2024), pp. 587–619.
[32]K. S. Cole and R. H. Cole, J. Chem. Phys. **9**(4), 341 (1941).
[33]J. Hunger, S. Niedermayer, R. Buchner, and G. Hefter, J. Phys. Chem. B **114**, 13617 (2010).
[34]T. Chen, G. Hefter, and R. Buchner, J. Phys. Chem. A **107**, 4025 (2003).
[35]U. Kaatze, J. Phys. Chem. **91**, 3111 (1987).
[36]C. Schröder and O. Steinhauser, J. Chem. Phys. **132**, 244109 (2010).
[37]J. M. Caillol, D. Levesque, and J. J. Weis, J. Chem. Phys. **91**, 5544 (1989).
[38]F. Alvarez, A. Alegra, and J. Colmenero, Phys. Rev. B **44**, 7306 (1991).
[39]Y. Kawasaki, H. Watanabe, and T. Uneyama, Nihon Reoroji Gakkaishi **39**, 127 (2011).
[40]R. Buchner, S. G. Capewell, G. Hefter, and P. M. May, J. Phys. Chem. B **103**, 1185 (1999).
[41]I. Rodríguez-Arteche, S. Cerveny, Á. Alegría, and J. Colmenero, Phys. Chem. Chem. Phys. **14**, 11352 (2012).
[42]V. Balos, S. Imoto, R. R. Netz, M. Bonn, D. J. Bonthuis, Y. Nagata, and J. Hunger, Nat. Commun. **11**, 1611 (2020).
[43]O. A. Dmitrieva, M. V. Fedotova, and R. Buchner, Phys. Chem. Chem. Phys. **19**, 20474 (2017).
[44]O. Blüh, Z. Phys. **25**, 220 (1924).
[45]N. Gavish and K. Promislow, Phys. Rev. E **94**, 012611 (2016).
[46]M. Neumann and O. Steinhauser, Chem. Phys. Lett. **106**, 563 (1984).
[47]C. Schröder and O. Steinhauser, J. Chem. Phys. **133**, 154511 (2010).
[48]C. Schröder, T. Sonnleitner, R. Buchner, and O. Steinhauser, Phys. Chem. Chem. Phys. **13**, 12240 (2011).
[49]M. Sega, S. Kantorovich, and A. Arnold, Phys. Chem. Chem. Phys. **17**, 130 (2015).
[50]R. A. X. Persson, Phys. Chem. Chem. Phys. **19**, 1982 (2017).
[51]E. Heid, B. Docampo-Álvarez, L. M. Varela, K. Prosenz, O. Steinhauser, and C. Schröder, Phys. Chem. Chem. Phys. **20**, 15106 (2018).
[52]Y. Nakayama, J. Colloid Interface Sci. **646**, 354 (2023).
[53]J. B. Hubbard, L. Onsager, W. M. Van Beek, and M. Mandel, Proc. Natl. Acad. Sci. U. S. A. **74**, 401 (1977).
[54]N. Ottosson, J. Hunger, and H. J. Bakker, J. Am. Chem. Soc. **136**, 12808 (2014).
[55]P. J. W. Debye, *Polar Molecules* (Dover Publications, New York, 1929).
[56]C. J. F. Böttcher and P. Borderwijk, *Theory of Electric Polarization* (Elsevier, Amsterdam, 1978), Vol. 1.
[57]A. Vila Verde and R. Lipowsky, J. Phys. Chem. B **117**, 10556 (2013).
[58]Q. Zhang, T. Wu, C. Chen, S. Mukamel, and W. Zhuang, Proc. Natl. Acad. Sci. U. S. A. **114**, 10023 (2017).
[59]M. González-Jiménez, Z. Liao, E. L. Williams, and K. Wynne, J. Am. Chem. Soc. **146**, 368 (2024).
[60]F. Pabst and S. Baroni, J. Phys. Chem. Lett. **16**, 7915 (2025).
[61]P.-M. Déjardin, F. Pabst, Y. Cornaton, A. Helbling, and T. Blochowicz, Phys. Rev. E **105**, 024108 (2022).
[62]V. Balos, M. Bonn, and J. Hunger, Phys. Chem. Chem. Phys. **17**, 28539 (2015).
[63]R. Buchner, J. Barthel, and J. Stauber, Chem. Phys. Lett. **306**, 57 (1999).
[64]D. Braun, S. Boresch, and O. Steinhauser, J. Chem. Phys. **140**, 064107 (2014).
[65]W. Wachter, W. Kunz, R. Buchner, and G. Hefter, J. Phys. Chem. A **109**, 8675 (2005).
[66]K. F. Rinne, S. Gekle, and R. R. Netz, J. Phys. Chem. A **118**, 11667 (2014).
[67]K. F. Rinne, S. Gekle, and R. R. Netz, J. Chem. Phys. **141**, 214502 (2014).
[68]Y. Feldman and P. Ben Ishai, "The microwave response of water as the measure of interactions in a complex liquid," in *Broadband Dielectric Spectroscopy: A Modern Analytical Technique*, ACS Symposium Series (American Chemical Society, 2021), Chap. 13, pp. 283–300.
[69]M. Neumann, J. Chem. Phys. **85**, 1567 (1986).
[70]P. Madden and D. Kivelson, Adv. Chem. Phys. **56**, 467 (1984).
[71]M. Neumann, J. Chem. Phys. **82**, 5663 (1985).
[72]P. Honegger, O. Steinhauser, and C. Schröder, J. Phys. Chem. Lett. **14**, 609 (2023).
[73]C. Schröder and O. Steinhauser, J. Phys.: Condens. Matter **28**, 344008 (2016).
[74]C. Schröder, T. Rudas, G. Neumayr, S. Benkner, and O. Steinhauser, J. Chem. Phys. **127**, 234503 (2007).
[75]J. M. Caillol, D. Levesque, and J. J. Weis, J. Chem. Phys. **85**, 6645 (1986).
[76]S. Chiacchiera, P. B. Warren, A. J. Masters, and M. A. Seaton, J. Chem. Phys. **161**, 174115 (2024).
[77]H.-N. Xu, Y. Liu, and L. Zhang, Soft Matter **11**, 5926 (2015).
[78]A. M. Hyde, S. L. Zultanski, J. H. Waldman, Y.-L. Zhong, M. Shevlin, and F. Peng, Org. Process Res. Dev. **21**, 1355 (2017).